PNAS RESEARCH ARTICLE | EARTH, ATMOSPHERIC, AND PLANETARY SCIENCES

Use of $\delta^{18}O_{atm}$ in dating a Tibetan ice core record of Holocene/Late Glacial climate

Lonnie G. Thompson[a,b,1], Jeffrey P. Severinghaus[c,1], Tandong Yao[d], Mary E. Davis[a], Ellen Mosley-Thompson[a,e], Emilie Beaudon[a], M. Roxana Sierra-Hernández[a], and Stacy E. Porter[f]

Contributed by Lonnie Thompson; received March 31, 2022; accepted September 23, 2022; reviewed by Amaëlle Landais and Laurence Yeung

Ice cores from the northwestern Tibetan Plateau (NWTP) contain long records of regional climate variability, but refrozen meltwater and dust in these cores has hampered development of robust timescales. Here, we introduce an approach to dating the ice via the isotopic composition of atmospheric O_2 in air bubbles ($\delta^{18}O_{atm}$), along with annual layer counting and radiocarbon dating. We provide a robust chronology for water isotope records ($\delta^{18}O_{ice}$ and d-excess) from three ice cores from the Guliya ice cap in the NWTP. The measurement of $\delta^{18}O_{atm}$, although common in polar ice core timescales, has rarely been used on ice cores from low-latitude, high-altitude glaciers due to (1) low air pressure, (2) the common presence of refrozen melt that adds dissolved gases and reduces the amount of air available for analysis, and (3) the respiratory consumption of molecular oxygen (O_2) by micro-organisms in the ice, which fractionates the $\delta^{18}O$ of O_2 from the atmospheric value. Here, we make corrections for melt and respiration to address these complications. The resulting records of water isotopes from the Guliya ice cores reveal climatic variations over the last 15,000 y, the timings of which correspond to those observed in independently dated lake and speleothem records and confirm that the Guliya ice cap existed before the Holocene. The millennial-scale drivers of $\delta^{18}O_{ice}$ are complex and temporally variable; however, Guliya $\delta^{18}O_{ice}$ values since the mid-20th century are the highest since the beginning of the Holocene and have increased with regional air temperature.

ice cores | northwestern Tibetan plateau | isotopes of atmospheric oxygen | Late Glacial | stable isotopes of ice

Significance

Ice cores drilled through the Guliya ice cap in northwestern Tibetan Plateau (NWTP) provide climate records dated using annual layer counting, radiocarbon dating, and the analysis of the isotopic composition of O_2 in air bubbles ($\delta^{18}O_{atm}$), a technique rarely used to date ice cores outside the polar regions. The high altitude of the ice cap, the presence of melt layers, and the effects of respiration by dust-hosted micro-organisms in the ice require the application of corrections to the Guliya $\delta^{18}O_{atm}$ values. These ice cores yield an ~15,000-y history of climate variability that resembles other stable isotope proxy records from both the TP and monsoon-dominated regions. The highest average $\delta^{18}O_{ice}$ value in the last ~12,000 y occurs after 1950 CE.

Outside the polar regions, the Tibetan Plateau (TP) contains Earth's largest frozen store of fresh water. Glaciers and ice fields on the TP and its bordering Himalayan range are major contributors to water resources in a region where a quarter of Earth's population lives. These glaciers feed the streams and rivers vital for agriculture, municipal water supplies, and hydropower, not only for nations in south and southeastern Asia but also for growing populations within the arid regions of the TP. Although recent precipitation trends have not been consistent across the TP, much of the region is experiencing widespread warming, which has had a detrimental effect on glaciers, particularly in the Himalayas (1, 2). The high-altitude glaciated areas of Asia are warming faster than the global average, and under the 1.5 °C global warming scenario, the glaciers in the mountains bordering the TP are projected to lose 50% of their area by 2100 CE (3).

The northwestern TP (NWTP) is a region of complex geomorphology and climatology where air masses from the Indian summer monsoon (ISM) and the continental westerlies interact (4–7) (Fig. 1*A*). Glaciers in the western Kunlun Mountains in the NWTP supply water to tributaries of the Tarim River, the longest inland river in China (Fig. 1*A*). This system supports the economically and agriculturally developing oases in the Tarim Basin (8). Until recently, glaciers of the western Kunlun Mountains were not experiencing noticeable mass loss; however, an assessment using satellite imagery from 2000 to 2019 shows that glaciers in the Karakoram and the NWTP began to recede in the late 2010s (9).

Ice cores recovered from TP glaciers have provided valuable histories of local and regional climatic and environmental variations that have helped place current anthropogenic-influenced changes in perspective. However, establishing the robust timescales required to reconstruct millennial-scale, ice core–derived paleohistories from the NWTP has proven to be difficult due to the low accumulation and lack of known time horizons (e.g., aerosols from dated volcanic eruptions). The measurement of the isotopic composition of oxygen in air bubbles in ice ($\delta^{18}O_{atm}$) is a well-established technique used to date ice cores from the polar regions (10–12). The advantage of using $\delta^{18}O_{atm}$ as a dating technique is that the variations through time are constant throughout the atmosphere because the mixing time of the atmosphere is only 1 y, while the isotopic

Author contributions: L.G.T., T.Y., E.M-T., and J.P.S. designed research; L.G.T., J.P.S., M.E.D and E.M-T. performed research; J.P.S. contributed new reagents/analytic tools; L.G.T., J.P.S. and M.E.D. analyzed data; and L.G.T., J.P.S., T.Y., M.E.D., E.M-T., E.B., M.R.S-H., and S.E.P. wrote the paper.

Reviewers: A.L., Laboratoire des Sciences du Climat et de l'Environnement; and L.Y., Rice University.

The authors declare no competing interest.

[1]To whom correspondence may be addressed. Email: jseveringhaus@ucsd.edu or thompson.3@osu.edu.

This article contains supporting information online at http://www.pnas.org/lookup/suppl/doi:10.1073/pnas.2205545119/-/DCSupplemental.

Published November 2, 2022.

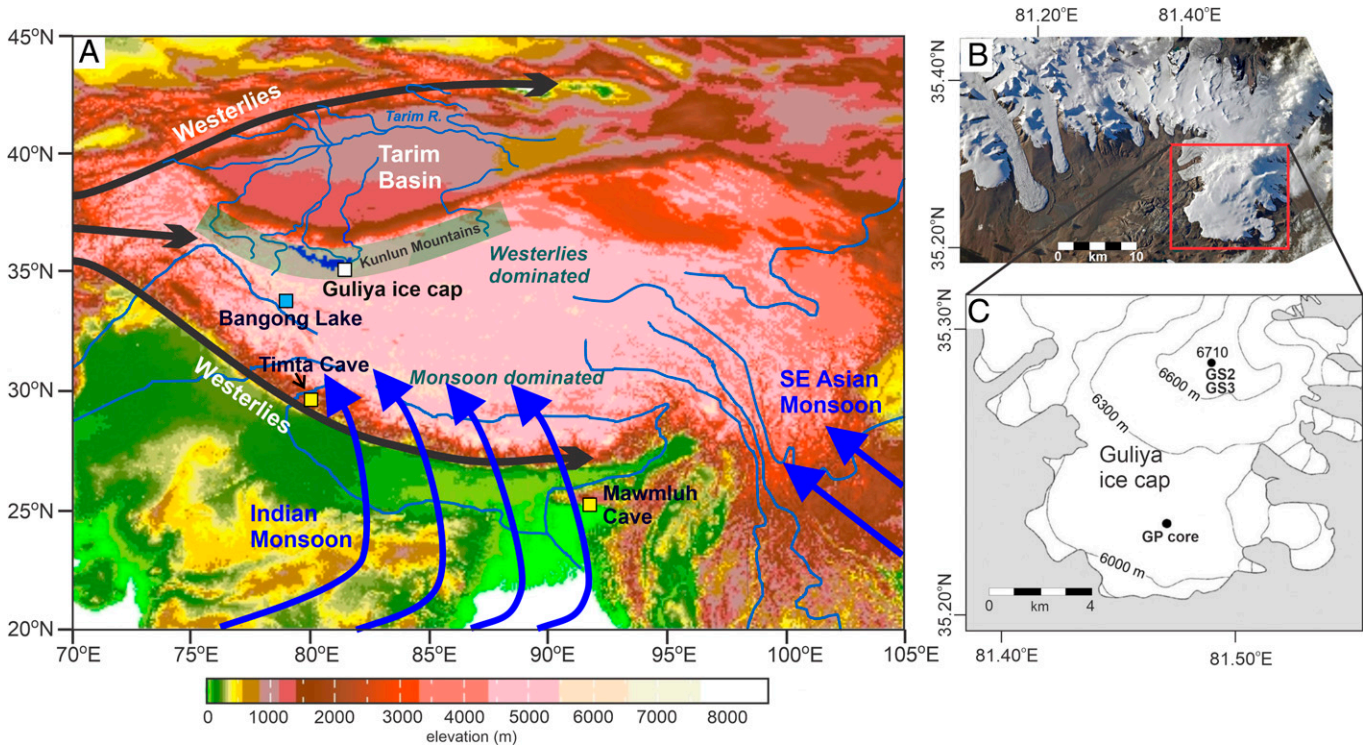

Fig. 1. Ice-core drill site locations on the Tibetan Plateau. (*A*) Relief map of the Tibetan Plateau showing the climate zones and movement of major air masses, along with the locations of the Guliya ice cap in the western Kunlun ice sheet (highlighted in blue), Bangong Lake, and the Timta and Mawmluh Caves. (*B*) Satellite image of the southeast sector of the western Kunlun ice sheet. The Guliya ice cap is outlined by the red box. (*C*) A topographic map shows the locations of the 2015 drill sites on the Guliya plateau (GP core) and the Guliya summit (GS2 and GS3). The 1992 drill site on the GP is in the vicinity of the 2015 site, although its location was not precisely fixed at the time of drilling (i.e., predates Global Positioning System use in China).

residence time of O_2 is ∼1,000 y (13). Therefore, the technique can be used to correlate ice-core records from the polar regions. This paper presents the use of $\delta^{18}O_{atm}$ to aid in the dating of ice cores from the Guliya ice cap in the western Kunlun Mountains in the NWTP (Fig. 1*A*). Here, the presence of melt and microbial respiration, which are not prevalent in polar glaciers and ice sheets, requires application of corrections to compensate for these processes. Gas-age measurements with the corrections applied are used to place the Guliya ice-core records in time and add an important technique for dating cores from glaciers throughout the data-sparse TP and the Himalayas.

Results

The Guliya Ice Core $\delta^{18}O_{ice}$ Records. To assess the relative magnitude of recent climate changes in this region within a longer-term perspective, a history of climate variability was reconstructed from ice cores drilled in 2015 through the Guliya ice cap (35.25°N; 81.48°E) on the south side of the western Kunlun Mountains (Fig. 1 *A* and *B*). Three cores were drilled to bedrock (50.72 m, 51.38 m, and 50.86 m) on the Guliya summit (GS) (6,710 masl), along with a core drilled to bedrock (309.7 m) at the Guliya Plateau (GP) site (6,200 masl) (Fig. 1*C*). Records of the $^{18}O/^{16}O$ ratio of ice ($\delta^{18}O_{ice}$) from two of the GS cores (GS2 and GS3) are shown with depth (Fig. 2*A*). The high degree of reproducibility between GS2 and GS3 indicates that the records are continuous and unaffected by stratigraphic anomalies. Despite their different elevations and glaciological settings (14), the GP core $\delta^{18}O_{ice}$ above 144.4 m depth (Fig. 2*B*) is broadly similar to the entire GS $\delta^{18}O_{ice}$ profiles. Although the GS drill sites (6,710 masl) are ∼500 m higher than the GP drill site and the borehole temperatures are lower (15), the $\delta^{18}O_{ice}$ averages of the two GS cores are unexpectedly higher than the average of the GP core. The cause of this relative ^{18}O enrichment at the higher elevation is unknown and may result from postdepositional processes, such as ventilation through the firn and/or wind scouring on the GS, or from the loss of summer snow by melting or sublimation on the GP. Unlike the cores from the GS that contain firn in their upper 25 m, the GP core is composed completely of ice below ∼1 m, indicating that snow converts to ice within a year of deposition.

Establishing the Timescale for the Guliya Ice Cores. The timescale was developed on the GS3 core using a variety of chronological techniques, including (1) annual layer counting in the upper 34 m of the GP core (15), which was transferred to GS3 by $\delta^{18}O_{ice}$ matching (*SI Appendix*, Fig. S1 and Table S1 and Section S1.1); (2) radiocarbon (^{14}C) dates of plant fragments from the GS2 and GP cores (*SI Appendix*, Table S2 and Section S1.2), also transferred to GS3 by $\delta^{18}O_{ice}$ matching; and (3) the $^{18}O/^{16}O$ ratio of atmospheric molecular oxygen ($\delta^{18}O_{atm}$) trapped in air bubbles in GS3. However, dating the core from the Guliya ice cap required application of corrections to the existing technique for measuring $\delta^{18}O_{atm}$. The use of $\delta^{18}O_{atm}$ in the polar regions takes advantage of the well-mixed nature of the atmosphere and the fact that the $^{18}O/^{16}O$ ratio of atmospheric dioxygen ($\delta^{18}O$ of O_2) changes in a known way over time, so that, in principle, all trapped-gas ice records should show the same curve (10–12). The traditional analysis of $\delta^{18}O_{atm}$ (i.e., without corrections) has been used successfully on three Andean cores (16–18), mainly to refine existing timescales that were constructed using other methods. However, this traditional technique has rarely been attempted on TP ice cores due to (1) low air pressure, (2) the common presence of refrozen melt that adds dissolved gases and reduces the amount of air available for analysis (*SI Appendix*, Fig. S2), and (3) the

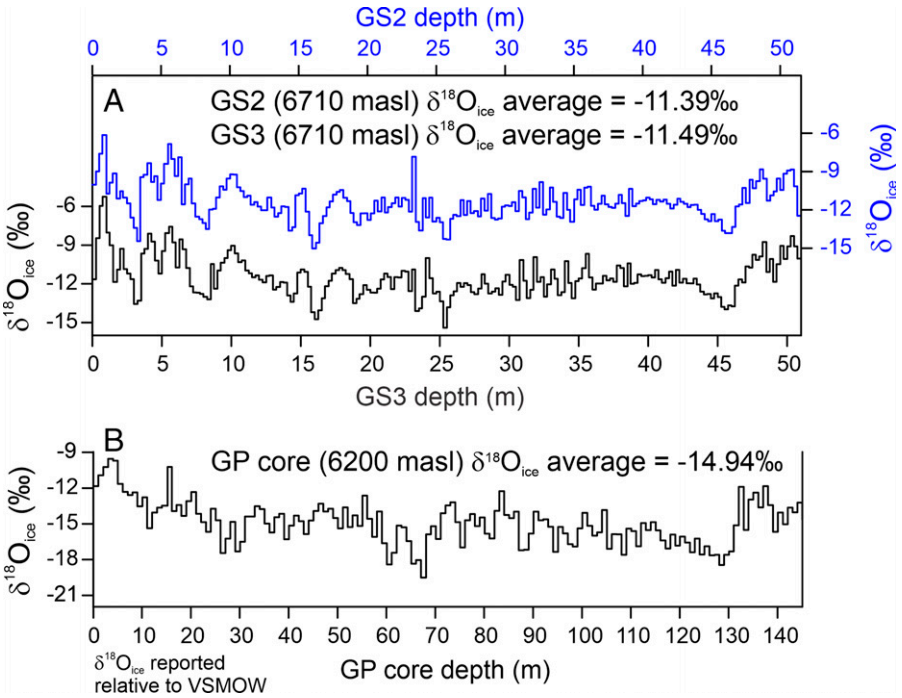

Fig. 2. $\delta^{18}O_{ice}$ profiles of Guliya ice cores in depth. (*A* and *B*) The $\delta^{18}O_{ice}$ records (*A*) from the Guliya summit cores (GS2 [blue] and GS3 [black]), both shown as 0.25-m averages, are compared with the $\delta^{18}O_{ice}$ record (*B*) from the GP core, shown as 1-m averages. The average $\delta^{18}O_{ice}$ values are shown; VSMOW indicates Vienna Standard Mean Ocean Water.

respiratory consumption of molecular oxygen by dust-hosted micro-organisms in the ice, which fractionates the $\delta^{18}O$ of O_2 from the atmospheric value.

Nineteen samples were cut from GS3 for $\delta^{18}O_{atm}$ analysis. In order to address the three challenges in determining $\delta^{18}O_{atm}$ in nonpolar ice listed above, corrections were applied to these samples as described in detail in Methods. To compensate for low air pressure, an inert gas (neon) was added to 13 of the 19 samples to increase the gas volume in the sample by a factor of five. The addition of neon was not required for six of the samples because they were cut at larger sizes. The other corrections involved (1) using the measured Ar/N_2 ratio to correct for the effects of melt, taking advantage of the fact that argon is twice as soluble as nitrogen in water, and (2) using the measured O_2/N_2 ratio to correct for the respiratory fractionation of the $\delta^{18}O$ of O_2.

The $\delta^{18}O_{atm}$ values obtained before the application of the corrections for melt and respiration fractionation are shown in *SI Appendix*, Table S3. The final calculated $\delta^{18}O_{atm}$ values (*SI Appendix*, Tables S4 and S5) are shown by depth in *SI Appendix* Fig. S3 and plotted with a West Antarctic ice sheet (WAIS) ice-core composite $\delta^{18}O_{atm}$ reference curve (19) (Fig. 3*A*). The ages of the 19 samples were determined from the match with the reference curve. An anomalously high value (1.466‰) at 49.35 m is most likely caused by excessive melting of the ice in the outer layer of the sample. A reference timescale was developed for the GS3 $\delta^{18}O_{ice}$ record by creating a fifth order polynomial function between −0.064 and 4.4 ka B.P. using the layer-counted ages and the ^{14}C dates and linear interpolations between the $\delta^{18}O_{atm}$-derived ages from GS3 samples that were older than the ^{14}C date of 4.4 ka B.P. (Fig. 3*B*). A composite of the GS3 and GS2 $\delta^{18}O_{ice}$ records based on the GS3 timescale was created (the GS composite), and this timescale was transferred to the GP core $\delta^{18}O_{ice}$ record by matching the water-isotopic profiles (*SI Appendix*, Fig. S4). The depth at which 15 ka B.P. occurs in the GP core is 144.4 m. This supports earlier findings (20) that the 308.6-m-long core drilled on the GP in 1992 contains a paleoclimate record extending beyond the Holocene, as does the 2015 GP core.

Discussion

The 2015 Guliya records are dated at much-higher resolution (100 y) than the $\delta^{18}O_{ice}$ record from the core drilled on the GP in 1992 (400 y) (20). The timescale is an improvement over the 1992 record, as it was constructed using independent dating techniques. In addition, unlike the 1992 Guliya ice core, deuterium excess (d-excess) was determined for each sample in the GS and GP cores, providing more information on climatic variations and moisture source since the end of the last deglaciation.

Several studies have been conducted that show correlations of varying significance between isotopic values in precipitation ($\delta^{18}O_{ppt}$) collected from across the TP and measured air temperatures during precipitation, especially north of 33°N (6, 21, 22). The modern-day temperature–$\delta^{18}O_{ppt}$ relationship has influenced the interpretation $\delta^{18}O_{ice}$ in TP glaciers as a proxy for air temperature over decadal to millennial timescales (15, 23–27). For example, *SI Appendix*, Fig. S5 shows increasing trends in average temperatures at several meteorological stations in the western TP from May to September, when ∼85% of the precipitation occurs, and annual averages of $\delta^{18}O_{ice}$ in the GP core. Whether the cause is the accelerated warming in the region or an intensification in the local moisture recycling due to glacier melting, the average $\delta^{18}O_{ice}$ from 1950 to 2014 CE is the highest since near the beginning of the Holocene (∼12 ka B.P., Fig. 4*A*), which is consistent with a construction of global mean surface temperature (28) that shows that current temperatures are the warmest in 11.3 ky.

The chronologies of the Guliya stable isotope records (Fig. 4 *A* and *B*) developed with the aid of $\delta^{18}O_{atm}$ are supported by similarities with an independently dated record of leaf wax δD from Bangong Lake (29) (Fig. 4*C*), located 300 km southwest of Guliya, and with speleothem records from northern India

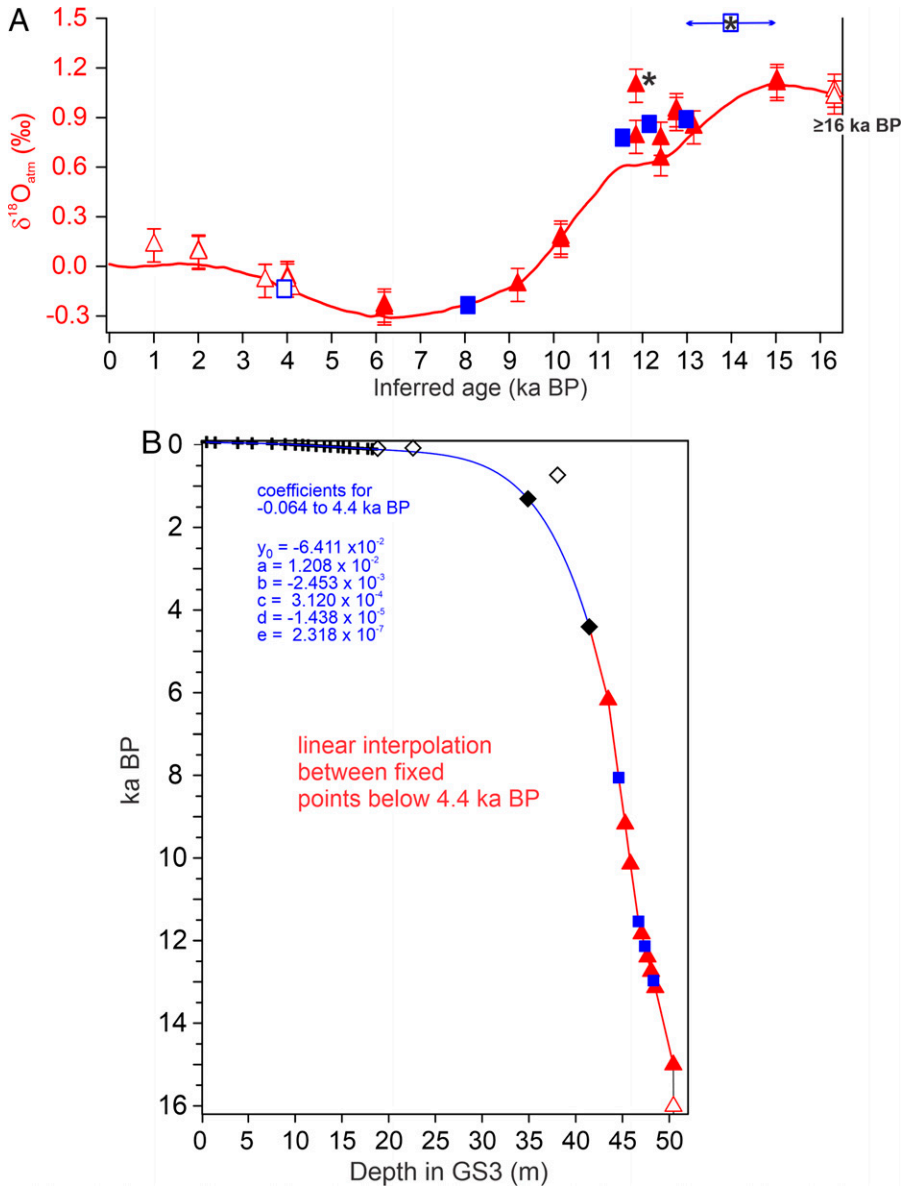

Fig. 3. Timescale reconstruction for GS3. (*A*) The inferred ages (ka B.P. or before 1950 CE) of 19 discrete samples (open and filled red triangles and open and filled blue squares) from GS3 (*SI Appendix*, Tables S4 and S5) were determined by the best fit between the general shape of the curve formed by their $\delta^{18}O_{atm}$ values at their respective depths (*SI Appendix*, Fig. S3) and the $\delta^{18}O_{atm}$ values from the WAIS (Antarctica) composite gas-age curve (19). The red triangles indicate $\delta^{18}O_{atm}$ values from samples to which neon was added to increase the volume of the gas; the blue squares indicate values from samples to which neon was not added. The $\delta^{18}O_{atm}$ value of 1.09 (closed red triangle) marked with a black asterisk may be an analytical artifact. The age of the anomalously high $\delta^{18}O_{atm}$ value of 1.466 (open blue square with black asterisk) can only be presented as a range based on the ages of the samples above and below it. (*B*) A fifth-order polynomial of depth versus age is constructed for GS3 from −0.65 to 4.4 ka B.P. using 18 layer counted dates (black crosses) (*SI Appendix*, Table S1) and two ^{14}C ages (black solid diamonds) (*SI Appendix*, Table S2). The open diamonds represent ^{14}C ages that were not used in the polynomial for reasons described in *Methods*. From 4.4 to 15 ka B.P., the age/depth relationship was calculated by linear interpolation between $\delta^{18}O_{atm}$ inferred ages of samples marked by filled red triangles and blue squares in (*A*). Since the inferred age of the $\delta^{18}O_{atm}$ value of 1.466‰ in (*A*) could not be specified, it was not included in (*B*).

(Timta and Mawmluh Caves) (30, 31) and from Oman (Qunf Cave) (32) (Fig. 4 *D* and *E*). These speleothem $\delta^{18}O$ records are interpreted as reflecting variations in intensity of the ISM, while the Bangong Lake δD record indicates variations in moisture source. Additionally, a composite of eastern China speleothem $\delta^{18}O$ records of Southeast Asian Monsoon activity (Hulu, Dongge, and Sanbao Caves) (33) (Fig. 4*F*) shows the same millennial-scale variations as the ice-core, lake, and ISM-isotope profiles. These similarities between the monsoon proxy records and the Guliya isotope records present complications in the interpretation of $\delta^{18}O_{ice}$ as temperature on millennial timescales, as the precession-driven movement of the monsoon front and the westerlies altered the contribution of different moisture sources to the NWTP. Studies of d-excess in glacier ice on the NWTP show that its value is determined largely by moisture source and pathways, i.e., higher/lower d-excess is determined by lower/higher monsoon contribution in the precipitation (34), which is similar to the relationship between δD in leaf wax in Bangong Lake and moisture source (29). If moisture source is a determining influence on d-excess in the NWTP glacier ice on millennial to precessional timescales, then the Guliya d-excess record potentially demonstrates the dominance of recycled westerly moisture before ∼12 ka B.P. followed by the influx of monsoon-derived moisture in the Early Holocene. This changing source resulted from the northward movement of the ISM across the TP toward the Kunlun Mountains (35).

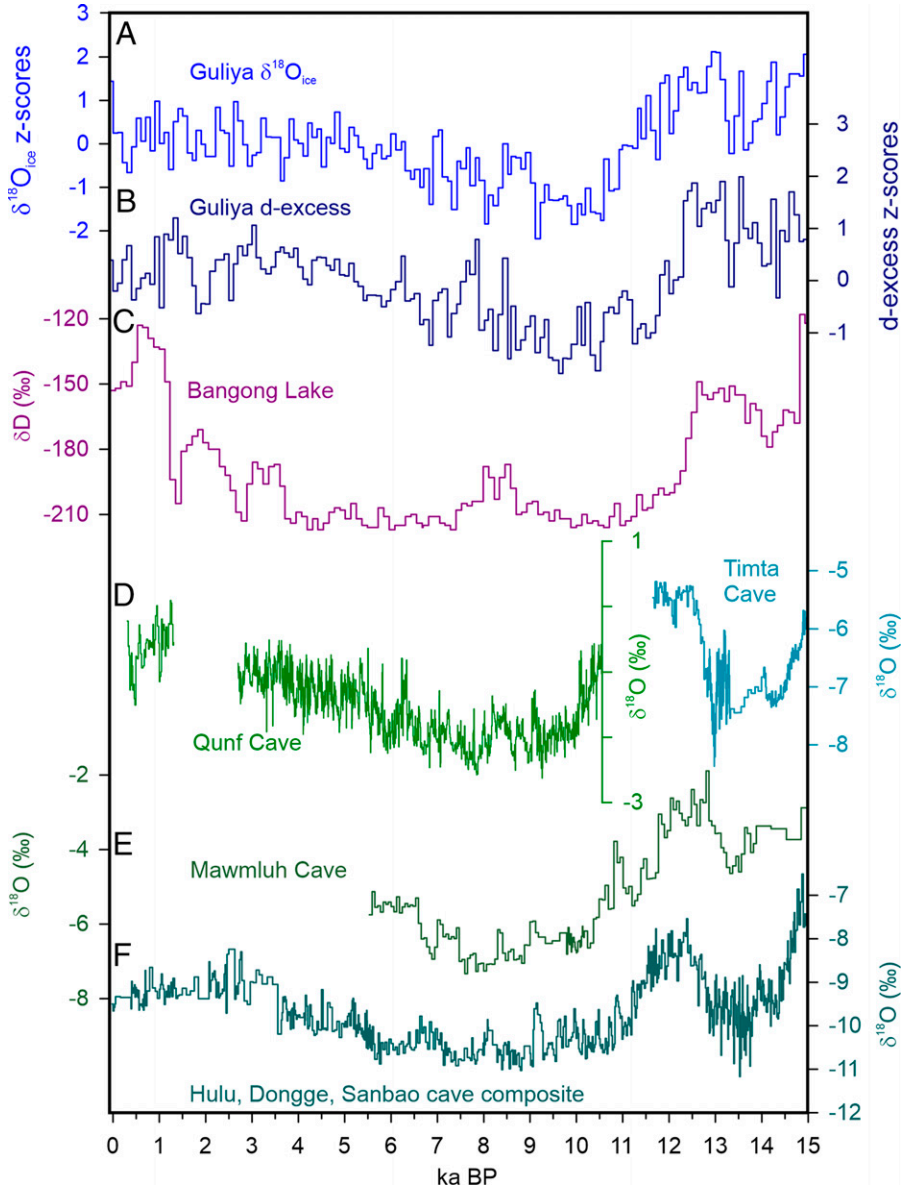

Fig. 4. Guliya 15 ky stable isotope records compared with monsoon proxy records. (*A* and *B*) Composites of GS2, GS3, GP (*A*) $\delta^{18}O_{ice}$, and (*B*) d-excess records, both shown as 100-y averages of z scores. (*C*) Leaf wax δD from Bangong Lake, western TP (29). (*D* and *E*) Speleothem $\delta^{18}O$ records illustrating ISM intensity from (*D*) Qunf Cave, Oman (17.17°N, 54.3°E) (32), Timta Cave (30) in the Indian Himalaya, and (*E*) Mawmluh Cave in northeast India (31). (*F*) Composite speleothem record (Dongge, Hulu, and Sanbao Caves) of Southeast Asian Monsoon intensity from eastern China (33).

Increasing trends in Guliya and speleothem isotopic records after ∼7 ka B.P. indicate a gradual transitioning to westerly sources as the monsoon front retreated to the south, interrupted by short periods of increased/decreased moisture contributed by monsoon/westerly airflow.

The striking similarities between the Guliya $\delta^{18}O_{ice}$ and the proxy records of moisture source/pathways and monsoon intensity over the last 15 ky indicate that the interpretation of oxygen isotopes in ice cores in the NWTP appears to be more complex than a straightforward correlation with temperature. Just as speleothem $\delta^{18}O$ can be determined by several processes, both local and distant (36, 37), $\delta^{18}O_{ice}$ in the NWTP can also be controlled by a combination of atmospheric and hydrospheric factors, such as monsoon and continental moisture sources, surface water temperature at the moisture source(s), recycling over water versus land, convective activity, and air temperature. The relative importance of each of these processes may have varied over the last 15 ky as the large Northern Hemisphere ice sheets retreated during the Late Glacial to the Middle Holocene and the monsoon front and westerlies shifted northward as summer insolation peaked in the Early Holocene and then gradually moved southward as insolation decreased.

Conclusions

The use of $\delta^{18}O_{atm}$ was instrumental in the construction of a timescale for climate records since the end of the Late Glacial from ice cores drilled through the Guliya ice cap in the NWTP. These records update and improve the previous Guliya Holocene chronology over this period, which did not have the advantage of independently dated time horizons. The corrections that were used to compensate for melt and respiration fractionation caused by the presence of micro-organisms in the ice should be useful for the development of millennial to processional-scale paleoclimate records from other high-altitude, nonpolar glaciers. This paper presents the application of these corrections.

The Guliya records challenge the interpretation of $\delta^{18}O_{ice}$ as influenced primarily by temperature in the northern TP, although temperature may play a major role as conditions change in the atmosphere and on land. In fact, the close relationship between temperature and precipitation stable isotopes that has been documented in recent decades may be influenced by other factors that were not previously present in the NWTP, such as the accelerating increase in atmospheric greenhouse-gas concentrations and rapidly expanding agriculture and urbanization in Central Asia and on the TP itself (38, 39). However, the relative importance of climatic and environmental processes on stable isotopes in precipitation in the past and ultimately archived in high-altitude glacier ice, such as Guliya at over 6,000 m above sea level, is beyond the scope of this paper.

Methods

Field and Laboratory. During the summer of 2015, three ice cores were drilled to bedrock on the summit of the Guliya ice cap (GS) and one core (referred to as the GP core) was drilled to bedrock on the lower GP. A shallow core (72.4 m) was also drilled on the GP near the deep core. Among the three GS cores, the first one drilled (GS1) was allocated to the Institute of Tibetan Plateau Research (ITP), the third core (GS3) was allocated to the Byrd Polar and Climate Research Center (BPCRC), and the second core (GS2) was split equally between the two institutions, as was the long GP core. All cores allocated to BPCRC were transported frozen to the cold-storage facility at The Ohio State University (OSU), where they are stored at −30 °C. The cores were analyzed for stable isotopes of oxygen ($\delta^{18}O_{ice}$) and hydrogen (δD_{ice}) on Picarro cavity ringdown spectrometers (L2120-i and L2140-i). Summit Core 3 (GS3, 50.86 m) was cut into 1,545 samples, and the GP core (309.7 m) was cut into 9,330 samples. The average precision for $\delta^{18}O_{ice}$ is 0.25‰, and for δD_{ice}, it is 0.80‰. Deuterium excess was calculated by the function [d-excess = $\delta D_{ice} - 8 \times \delta^{18}O_{ice}$].

Melt and Respiratory Corrections for $\delta^{18}O_{atm}$. It is important to note that the classical calculation of $\delta^{18}O_{atm}$, $\delta^{18}O - 2 \times \delta^{15}N$ (*SI Appendix*, Table S3), already approximately corrects for any kinetic fractionation that may have occurred during the rapid dissolution of gas into the liquid water, in addition to the classical 2:1 gravitational correction. The reason is that $\delta^{18}O$ of O_2 is roughly twice as fractionated by disequilibrium ($\varepsilon_{18} = -2.8 \pm 0.2$‰) as is $\delta^{15}N$ of N_2 ($\varepsilon_{15} = -1.3 \pm 0.1$‰) (40). Using the following input parameters for gases at 0 °C: O_2 solubility = 0.4572 mol/m^3/atm moist air, Ar solubility = 0.0223 mol/m^3/atm moist air, and N_2 solubility = 0.8304 mol/m^3/atm moist air (41), we next take a more-quantitative approach to calculating the melt and respiration amounts in order to make robust corrections to the data.

For the local barometric pressure at GS of 0.472 atm (~6,000 m elevation),

O_2/N_2 ratio of standard gas = 0.26826
Ar/N_2 ratio of standard gas = 0.01196
Mole fraction N_2: 0.78080, O_2: 0.20946, Ar: 0.00934, other: 0.00040

First, we calculate the melt fraction from the measured Ar/N_2 ratio and the solubilities of Ar and N_2. The melt fraction is conceptualized as the ratio of refrozen melt volume to the sum of the equivalent air bubble volume (at 0 °C, 0.472 atm) and the melt volume:

$$\text{Melt fraction} \equiv \frac{\text{melt volume}}{\text{bubble + melt volume}} = \frac{1}{\frac{\text{bubble vol}}{\text{melt vol}} + 1} = f_m. \quad [1]$$

In this conceptualization, a melt fraction of 1 means there are no air bubbles. The measured Ar/N_2 ratio in the sample is assumed to reflect the contributions from air bubbles and dissolved gases in the melt:

$$Ar/N_{2measured} = \left(\frac{\delta Ar/N_2}{1000} + 1\right) Ar/N_{2\ standard\ gas} = \frac{Ar_{bub} + Ar_{melt}}{N_{2bub} + N_{2melt}} = \frac{Ar_{air}V_{bub} + S_{Ar}P_{air}V_{melt}}{N_{2air}V_{bub} + S_{N2}P_{air}V_{melt}},$$

where Ar_{air} = moles of Ar per m^3 of air at 0 °C and 0.472 atm;
N_{2air} = moles of N_2 per m^3 of air at 0 °C and 0.472 atm;
V_{bub} = volume of bubbles in sample, 0 °C equivalent (1% more than volume at −2.73 °C);
S_{Ar} = solubility of Ar at 0 °C;
S_{N2} = solubility of N_2 at 0 °C;
P_{air} = air pressure, 0.472 atm;
and V_{melt} = volume of melted and refrozen ice in sample.

Rearranging and solving for the ratio V_{bub}/V_{melt},

$$Ar/N_{2meas}N_{2air}V_{bub} - Ar_{air}V_{bub} = S_{Ar}P_{air}V_{melt} - Ar/N_{2meas}S_{N2}P_{air}V_{melt}$$
$$\frac{V_{bub}}{V_{melt}} = \frac{\{S_{Ar}P_{air} - Ar/N_{2meas}S_{N2}P_{air}\}}{\{Ar/N_{2meas}N_{2air} - Ar_{air}\}}.$$

Substituting (Eq. **2**) into (Eq. **1**) gives the melt fraction (*SI Appendix*, Fig. S2):

$$\text{Melt fraction } f_m = \frac{1}{\frac{S_{Ar}P_{air} - Ar/N_{2meas}S_{N2}P_{air}}{Ar/N_{2meas}N_{2air} - Ar_{air}} + 1}.$$

The next step is to calculate the apparent "missing O_2" from the difference between measured O_2 and expected O_2 from the Ar-based melt estimate (using the ratio of their solubilities). This calculation assumes that any disequilibrium has affected Ar and O_2 similarly. This missing O_2 is assumed to reflect respiratory consumption, enabling a correction for the well-known respiratory isotope fractionation of $\delta^{18}O$. The missing O_2 is expressed as a fraction f_{resp}, which is the amount respired divided by the initial dissolved O_2 amount:

$$f_{resp} = \frac{[O_{2air}(1-f_m) + S_{O2}P_{air}f_m - O_2/N_{2meas}N_{2air}(1-f_m) - O_2/N_{2meas}S_{N2}P_{air}f_m]}{S_{O2}P_{air}f_m}$$

where

$$O_2/N_{2meas} = \left(\frac{\delta O_2/N_2}{1000} + 1\right) O_2/N_{2\ standard\ gas}.$$

The remaining O_2 is expressed as a fraction (f_{O2}) of the total O_2 in the sample:

$$f_{O2} = \frac{(1 - f_{resp})S_{O2}P_{air}f_m}{O_{2air}(1 - f_m) + (1 - f_{resp})S_{O2}P_{air}f_m}.$$

The isotope fractionation $\Delta\delta$ is assumed to have a Rayleigh-type dependence $f^{\alpha-1}$ on the fraction f of the initial amount that remains, where α is the respiratory fractionation factor (42). Equilibrium solubility fractionation ε_{18sol} and ε_{15sol} of the isotopes of O_2 and N_2 is also included (43):

$$\Delta\delta^{18}O = \left\{\left[(1 - f_{resp})^{\alpha-1} - 1\right]1000‰ + \varepsilon_{18sol}\right\}f_{O2} - 2\ \Delta\delta^{15}N_{sol}$$
$$\Delta\delta^{15}N_{sol} = \frac{\delta_{15sol}S_{N2}P_{air}f_m}{[N_{2air}(1 - f_m) + S_{N2}P_{air}f_m]}.$$

Unfortunately, the actual value of α in melted snow containing dust and micro-organisms is not known a priori. Measured values in natural ecosystems range from roughly 0.973 to 0.993 (43) and largely depend on the degree to which the respiratory system is well mixed internally, with weaker net fractionation occurring when the system is poorly mixed or respiration is limited by diffusive transport (44).

To proceed, we let α be an adjustable parameter and force the $\delta^{18}O$-based chronology to fit a measured radiocarbon date of 4.4 ka B.P. at ~41.5 m. This results in a value of 0.99 for α. This is a reasonable value, given the very slow diffusion rate of O_2 in liquid water (~10^{-5} cm/s) and the likelihood that O_2 may have been strongly consumed in the immediate vicinity of dust grains, where micro-organisms are known to be concentrated, causing consumption of isotopically enriched O_2 and thus less overall $\delta^{18}O$ increase. An α value of 0.99 has been found in waterlogged tropical soils (45), which also have very slow O_2 diffusion rates. We note that many of the $\delta^{18}O_{atm\text{-}m\&r}$ points fall slightly above the reference curve, suggesting that the value of α may vary. This is unsurprising, given the known variation in α measured in soils (42), and is expected, due to the fact that the ice is not an internally well-mixed environment for O_2, causing net fractionation to be partly due to diffusion rather than respiratory enzymatic fractionation.

The final correction to the classical $\delta^{18}O_{atm}$ value for melt and respiration is

$$\delta^{18}O_{atm\_m\&r} = \delta^{18}O_{atm} - \Delta\delta^{18}O.$$

All calculated values are given in *SI Appendix*, Tables S4 and S5. The final $\delta^{18}O_{atm}$ values that are shown plotted with depth in *SI Appendix*, Fig. S3 were fitted to the WAIS $\delta^{18}O_{atm}$ reference curve (19) using Analyseries software (46).

The $\delta^{18}O_{atm}$ values of the last two samples in *SI Appendix*, Table S3 (GS3-T51, 52) are much larger (+1.4‰) than the known maximum value of +1.2‰ for the atmosphere during the past >800 ky (47), suggesting that the samples have been enriched in ^{18}O by some fractionation process in the Guliya snowpack. Because the atmospheric residence time of O_2 is ∼1,000 y (13) and the atmospheric mixing time is ∼1 y, these values cannot be representative of the true atmosphere. The high values of Ar/N_2 (+120‰) in sample GS3-T52 also suggest a large component of melt, and the low total air content (0.008 mlSTP/g) confirms that conclusion. Because ^{18}O is slightly more soluble in water than ^{16}O (isotope fractionation, or $\varepsilon = +0.833$ at 0 °C) (43), the melt could have contributed slightly to the high $\delta^{18}O_{atm}$ values. Yet, despite the fact that O_2 and Ar have very similar solubilities, the lower O_2/N_2 (∼+50‰) relative to Ar/N_2 suggests a major loss of oxygen, probably by respiration (argon as a noble gas cannot be consumed by respiration). It is evident that both melting and respiration have occurred, which increase $\delta^{18}O_{atm}$ (48). However, after the application of corrections for melt and respiration fractionation (*SI Appendix*, Table S4), the data points below 50 m fit with the WAIS reference curve (Fig. 3*A*), which appears to capture the well-known 15 ka B.P. atmospheric $\delta^{18}O$ maximum. This feature is a unique extremum that makes for an unambiguous dating target (19, 48).

Data, Materials, and Software Availability. The data presented in this study (raw data of stable isotopes of oxygen ($\delta^{18}O_{ice}$) and deuterium excess and 100-y averages) are archived at the National Oceanic and Atmospheric Administration World Data Service for Paleoclimatology: study/36913 https://www.ncdc.noaa.gov/paleo-search/study/XXXX (49-50).

ACKNOWLEDGMENTS. We thank all the field personnel who supported the activities associated with drilling the Guliya cores in 1992 and 2015 and those who contributed to the analyses of the cores. We especially thank Dr. Ping-Nan Lin (BPCRC) for the $\delta^{18}O_{ice}$ measurements. We thank the Woods Hole National Ocean Sciences Accelerator Mass Spectrometry facility and Jürg Beer and Hans-Arno Synal at the Swiss Federal Institute of Technology for ^{14}C analysis of plant material from the Guliya ice cores. Ross Beaudette of the Scripps Institution of Oceanography provided lab support. We also thank Anil Gupta at the Indian Institute of Technology Kharagpur for the Mawmluh Cave speleothem data. This project was funded by U.S. NSF P2C2 Award 1502929 and the Institute of Theoretical Physics, Chinese Academy of Sciences. This is Byrd Polar and Climate Research Center contribution No. C-1598.

Author affiliations: [a]Byrd Polar and Climate Research Center, The Ohio State University, Columbus, OH 43210; [b]School of Earth Sciences, The Ohio State University, Columbus, OH 43210; [c]Scripps Institution of Oceanography, University of California, San Diego, CA 92093; [d]Key Laboratory of Tibetan Climate Changes and Land Surface Processes, Institute of Tibetan Plateau Research, Chinese Academy of Sciences, Beijing 100864, China; [e]Department of Geography, The Ohio State University, Columbus, OH 43210; and [f]Department of Biological and Environmental Sciences, Wittenberg University, Springfield, OH 45501

1. T. Bolch *et al.*, The state and fate of Himalayan glaciers. *Science* **336**, 310–314 (2012).
2. T. Yao *et al.*, Different glacier status with atmospheric circulations in Tibetan Plateau and surroundings. *Nat. Clim. Chang.* **2**, 663–667 (2012).
3. P. D. A. Kraaijenbrink, M. F. P. Bierkens, A. F. Lutz, W. W. Immerzeel, Impact of a global temperature rise of 1.5 degrees Celsius on Asia's glaciers. *Nature* **549**, 257–260 (2017).
4. C. P. Chang, P. Harr, J. Ju, Possible roles of Atlantic circulations on the weakening Indian monsoon rainfall-ENSO relationship. *J. Clim.* **14**, 2376–2380 (2001).
5. S. Feng, Q. Hu, How the North Atlantic Multidecadal Oscillation may have influenced the Indian summer monsoon during the past two millennia. *Geophys. Res. Lett.* **35**, L01707 (2008).
6. T. Yao *et al.*, A review of climatic controls on $\delta^{18}O$ in precipitation over the Tibetan Plateau: Observations and simulations. *Rev. Geophys.* **51**, 525–548 (2013).
7. J. Curio, F. Maussion, D. Scherer, A twelve-year high-resolution climatology of atmospheric water transport over the Tibetan Plateau. *Earth Syst. Dyn.* **6**, 109–124 (2015).
8. M. Disse, Sustainable land and water management of river oases along the Tarim River. *Proc. IAHS* **93**, 1–5 (2016).
9. R. Hugonnet *et al.*, Accelerated global glacier mass loss in the early twenty-first century. *Nature* **592**, 726–731 (2021).
10. M. Bender *et al.*, Climate correlations between Greenland and Antarctica during the past 100,000 years. *Nature* **372**, 663–666 (1994).
11. E. J. Brook *et al.*, Timing of millennial-scale climate change at Siple Dome, West Antarctica, during the last glacial period. *Quat. Sci. Rev.* **24**, 1333–1343 (2005).
12. A. Landais *et al.*, The glacial inception as recorded in the NorthGRIP Greenland ice core: Timing, structure and associated abrupt temperature changes. *Clim. Dyn.* **26**, 273–284 (2006).
13. J. P. Severinghaus, R. Beaudette, M. A. Headly, K. Taylor, E. J. Brook, Oxygen-18 of O_2 records the impact of abrupt climate change on the terrestrial biosphere. *Science* **324**, 1431–1434 (2009).
14. S. Kutuzov, L. G. Thompson, I. Lavrentiev, L. Tian, Ice thickness measurements of Guliya ice cap, western Kunlun Mountains (Tibetan Plateau), China. *J. Glaciol.* **64**, 977–989 (2018).
15. L. G. Thompson *et al.*, Ice core records of climate variability on the Third Pole with emphasis on the Guliya ice cap, western Kunlun Mountains. *Quat. Sci. Rev.* **188**, 1–14 (2018).
16. L. G. Thompson *et al.*, A 25,000-year tropical climate history from Bolivian ice cores. *Science* **282**, 1858–1864 (1998).
17. E. Ramirez *et al.*, A new Andean deep ice core from Nevado Illimani (6350 m), Bolivia. *Earth Planet. Sci. Lett.* **212**, 337–350 (2003).
18. M. E. Davis, L. G. Thompson, An Andean ice-core record of a Middle Holocene mega-drought in North Africa and Asia. *Ann. Glaciol.* **43**, 34–41 (2006).
19. A. M. Seltzer *et al.*, Does $\delta^{18}O$ of O_2 record meridional shifts in tropical rainfall? *Clim. Past* **13**, 1323–1338 (2017).
20. L. G. Thompson *et al.*, Tropical climate instability: The last glacial cycle from a Qinghai-Tibetan ice core. *Science* **276**, 1821–1825 (1997).
21. Z. Pang *et al.*, Processes affecting isotopes in precipitation of an arid region. *Tellus B Chem. Phys. Meterol.* **63**, 352–359 (2011).
22. G. Juan *et al.*, Environmental effect and spatiotemporal pattern of stable isotopes in precipitation on the transition zone between the Tibetan Plateau and arid region. *Sci. Total Environ.* **749**, 141559 (2020).
23. S. Kang, D. Qin, P. A. Mayewski, C. P. Wake, J. Ren, Climatic and environmental records from the Far East Rongbuk ice core, Mt. Qomolangma (Mt. Everest). *Episodes* **24**, 176–181 (2001).
24. N. Wang, T. Yao, L. G. Thompson, M. E. Davis, Strong negative correlation between dust event frequency and air temperature over the northern Tibetan Plateau reflected by the Malan ice-core record. *Ann. Glaciol.* **43**, 29–33 (2006).
25. W. An *et al.*, Possible recent warming hiatus on the northwestern Tibetan Plateau derived from ice-core records. *Sci. Rep.* **6**, 32813 (2016).
26. H. Pang *et al.*, Temperature trends in the northwestern Tibetan Plateau constrained by ice core water isotopes over the past 7,000 years. *J. Geophys. Res.* **125**, e2020JD032560 (2020).
27. W. Yu *et al.*, Temperature signals of ice core and speleothem isotopic records from Asian monsoon region as indicated by precipitation $\delta^{18}O$. *Earth Planet. Sci. Lett.* **554**, 116665 (2020).
28. S. A. Marcott, J. D. Shakun, P. U. Clark, A. C. Mix, A reconstruction of regional and global temperature for the past 11,300 years. *Science* **339**, 1198–1201 (2013).
29. J. Hou, W. J. D'Andrea, M. Wang, Y. He, J. Liang, Influence of the Indian monsoon and the subtropical jet on climate change on the Tibetan Plateau since the late Pleistocene. *Quat. Sci. Rev.* **163**, 84–94 (2017).
30. A. Sinha *et al.*, Variability of southwest Indian summer monsoon precipitation during the Bølling-Ållerød. *Geology* **33**, 813–816 (2005).
31. S. Dutt, A. K. Gupta, B. Wünnemann, D. Yan, Abrupt changes in Indian summer monsoon strength during 33,800 to 5000 years B.P. *Geophys. Res. Lett.* **42**, 5526–5532 (2015).
32. D. Fleitmann *et al.*, Holocene forcing of the Indian monsoon recorded in a stalagmite from southern Oman. *Science* **300**, 1737–1739 (2003).
33. H. Cheng *et al.*, The Asian monsoon over the past 640,000 years and ice age terminations. *Nature* **534**, 640–646 (2016).
34. W. An *et al.*, Enhanced recent local moisture recycling on the northwestern Tibetan Plateau deduced from ice core deuterium excess records. *J. Geophys. Res. Atmos.* **122**, 12,541–12,556 (2017).
35. A. Ramisch *et al.*, A persistent northern boundary of Indian Summer Monsoon precipitation over Central Asia during the Holocene. *Sci. Rep.* **6**, 25791 (2016).
36. J. Hu, J. Emile-Gaey, C. Tabor, J. Nusbaumer, J. Partin, Deciphering oxygen isotope records from Chinese speleothems with an isotope-enabled climate model. *Paleoceanogr. Paleoclimatol.* **34**, 2098–2112 (2019).
37. A. Baker *et al.*, Global analysis reveals climatic controls on the oxygen isotope composition of cave drip water. *Nat. Commun.* **10**, 2984 (2019).
38. L. Chen, W. Yu, F. Han, Y. Lu, T. Zhang, Effects of desertification on permafrost environment in Qinghai-Tibetan Plateau. *J. Environ. Manage.* **262**, 110302 (2020).
39. W. Luan, X. Li, Rapid urbanization and its driving mechanism in the Pan-Third Pole region. *Sci. Total Environ.* **750**, 141270 (2021).
40. M. Knox, P. D. Quay, D. Wilbur, Kinetic isotopic fractionation during air-water gas transfer of O_2, N_2, CH_4, and H_2. *J. Geophys. Res.* **97**, 20,335–20,343 (1992).
41. R. C. Hamme, D. P. Nicholson, W. J. Jenkins, S. R. Emerson, Using noble gases to assess the ocean's carbon pumps. *Annu. Rev. Mar. Sci.* **11**, 75–103 (2019).
42. A. Angert, M. Rodeghiero, K. Griffin, High alternative oxidase activity in cold soils and its implication to the Dole Effect. *Geophys. Res. Lett.* **39**, L16710 (2012).
43. B. B. Benson, D. Krause, Jr, The concentration and isotopic fractionation of oxygen dissolved in freshwater and seawater in equilibrium with the atmosphere. *Limnol. Oceanogr.* **29**, 620–632 (1984).
44. B. Luz, E. Barkan, The isotopic composition of atmospheric oxygen. *Global Biogeochem. Cycles* **25**, GB3001 (2011).
45. A. Angert *et al.*, Contribution of soil respiration in tropical, temperate, and boreal forests to the ^{18}O enrichment of atmospheric O_2. *Global Biogeochem. Cycles* **17**, 1089 (2003).
46. D. Paillard, L. Labeyrie, P. You, Analyseries 1.0: A Macintosh software for the analysis of geographical time-series. *Eos (Wash. D.C.)* **77**, 379 (1996).
47. A. Landais *et al.*, What drives the millennial and orbital variations of $\delta^{18}O_{atm}$? *Quat. Sci. Rev.* **29**, 235–246 (2010).
48. M. Bender, T. Sowers, L. Labeyrie, The Dole effect and its variations during the last 130,000 years as measured in the Vostok ice core. *Global Biogeochem. Cycles* **8**, 363–376 (1994).
49. L. G. Thompson *et al.*, GuliyaIceCores_2015, Dataset: Guliya2015_raw_d18O_dex.txt, https://www.ncei.noaa.gov/access/paleo-search/study/36913. Deposited 7 October 2022.
50. L. G. Thompson *et al.*, GuliyaIceCores_2015, Dataset: Guliya2015_100yavgs_d18O_dex.txt, https://www.ncei.noaa.gov/access/paleo-search/study/36913. Deposited 7 October 2022.